ELSEVIER

Nuclear Instruments and Methods in Physics Research B 191 (2002) 549–558

NIM B
Beam Interactions with Materials & Atoms

www.elsevier.com/locate/nimb

Radiation induced amorphization resistance in A_2O_3–BO_2 oxides

Kurt E. Sickafus [a,*], James A. Valdez [a], Jesse R. Williams [a], Robin W. Grimes [b], Heather T. Hawkins [c]

[a] *Materials Science and Technology Division, Los Alamos National Laboratory, Mail-Stop G755, Los Alamos, NM 87545, USA*
[b] *Department of Materials, Imperial College, Prince Consort Road, London SW7 2BP, UK*
[c] *Nuclear Materials and Technology, Los Alamos National Laboratory, Mail-Stop E574, Los Alamos, NM 87545, USA*

Abstract

Much work has been devoted in recent years to identifying ceramic materials that can withstand high doses of radiation without incurring excessive defect accumulation, or suffering undesirable transformations such as amorphization. In this paper, it is proposed that a large range of A_2O_3–BO_2 oxide compositions, with structures related to the fluorite crystal structure, may exhibit exceptional resistance to radiation-induced amorphization. Results of heavy ion irradiations on selected A_2O_3–BO_2 oxide compounds are presented in support of this prediction. © 2002 Elsevier Science B.V. All rights reserved.

PACS: 61.80.Jh; 81.05.Je; 61.82.Ms; 61.16.Bg; 61.80.Az

1. Introduction

There has been growing interest in recent years in radiation tolerant ceramics, whose potential applications range from nuclear fuel forms (see for example [1]), to nuclear waste forms (see for example [2]), to insulators for fusion reactor diagnostics (see for example [3–5]). Though numerous criteria can be defined to assess radiation tolerance, resistance to amorphization is widely accepted as a *necessary* (albeit not necessarily sufficient) materials' design criterion. Amorphization resistance is important because radiation-induced amorphization transformations are usually accompanied by large and undesirable volume changes, as well as changes in mechanical properties (see for example [6]). In a previous report, we proposed that a large variety of $A_2B_2O_7$ oxide compositions may exhibit resistance to amorphization [7]. In this paper, we present evidence indicating that the range of oxide compositions which may offer this desirable behavior, extends far beyond the so-called 227 pyrochlore compositions indicated above.

2. Experimental procedure

A_2O_3 and BO_2 powders from Alfa Aesar (99.99–99.999% purity) were used to produce pure A_2O_3 and BO_2 oxide sintered pellets, as well as A_2O_3–BO_2 mixtures. The specific compounds discussed in

* Corresponding author. Fax: +1-505-667-6802.
E-mail address: kurt@lanl.gov (K.E. Sickafus).

0168-583X/02/$ - see front matter
PII: S0168-583X(02)00609-2

Table 1
Selected structural data along with ion range and displacement damage parameters for Xe^{++} ion irradiations of Dy_2O_3 and $Y_2Ce_2O_7$

Compound	Measured lattice parameter (based on powder X-ray diffraction) (nm)	Theoretical density (g/cm^3)	Xe^{++} ion energy (keV)	Ion range (nm)	Ion longitudinal straggling (nm)	Depth of the peak in the displacement damage profile (nm)	Peak displacement damage dose at ion fluence 1×10^{20} Xe/m^2 (dpa)
Dy_2O_3	1.0665	7.81	300	66	29	33	44
$Y_2Ce_2O_7$	0.53827	6.07	350	75	30	45	36

Calculations performed using the Monte Carlo simulation program SRIM-2000 [22], assuming a displacement threshold energy of 40 eV for all target atoms (arbitrary assumption), dpa: displacement damage dose in units of displacements per atom.

this paper are Dy_2O_3 and $Y_2Ce_2O_7$. Powders were ball-milled in a SPEX mill with zirconia balls in a zirconia vial for ~1.5 h. Pellets with a mass of ~4 g were cold-pressed in a 13 mm diameter die, either dry ($Y_2Ce_2O_7$) or using ethylene glycol as a lubricant (Dy_2O_3). Samples were held for approximately 3 min at a cold-pressing pressure ranging from 3 to 7 metric tons. Green densities obtained by these procedures were typically 70% of theoretical. In the case of lubricated Dy_2O_3 pellets, the lubricant was burnt off at a temperature of ~570 K for a period of 12 h. These Dy_2O_3 samples were pre-sintered at 1620 K for 36 h, then ground and pressed for final sintering at 1870 K for 25 h. $Y_2Ce_2O_7$ samples were annealed at 870 K for 1 h, ground and pressed and annealed a second time at 1570 K for 50 h, then ground and pressed and annealed for a final time at 1670 K for 8 h, then increasing the temperature to 1870 K for 60 h. Final sintered densities ranged from 85–95% of theoretical.

Samples were cut into discs 0.5 mm thick and polished to a mirror finish, in preparation for ion irradiation. Ion irradiations were performed in the Ion Beam Materials Laboratory (IBML) at Los Alamos National Laboratory, using an ion implanter operating at 150–175 kV. 300–350 keV Xe^{++} ions were implanted using a ion flux of between $3–4 \times 10^{16}$ Xe/m^2 s with the target at cryogenic temperature (100 K). Ion fluences in these experiments ranged from 1×10^{18}–5×10^{20} Xe/m^2. Table 1 shows ion range and displacement damage parameters for experimental conditions used in this study.

Irradiated samples were prepared in cross-sectional geometry for examination using transmission electron microscopy (TEM). Final thinning to electron transparency was accomplished using 5 keV Ar^+ ion milling. Samples were then coated with a thin layer of carbon to prevent charging problems during TEM analysis. Samples were analyzed by TEM using a Philips CM-30 microscope operating at 300 kV.

3. Results

3.1. Crystal chemistry perspective

Fig. 1 shows a schematic representation for A_2O_3–BO_2 compounds that we propose may be of interest in the search for radiation tolerant oxide ceramics. In the drawings in Fig. 1, the vertical axis in the front of each drawing indicates increasing B^{4+} ionic radius, while the horizontal axis in the back represents increasing A^{3+} radius. The additional edges in each drawing inscribe a faceted volume that is best described as two trigonal prisms, rotated by 90° and joined on a central, square face.

The front vertical axis (Fig. 1(a)) is meant to represent pure BO_2 compounds with increasing B^{4+} radii from bottom to top. Ti^{4+} is the smallest cation along this axis, with $Ti^{4+}(VI)$ [1] = 0.0605 nm for the rutile polymorph of this compound (ionic radii in this report based on Shannon [8]). The largest cation along this axis is $Ce^{4+}(VIII) = 0.0970$ nm, in the fluorite-structured compound CeO_2. Between these are $Hf^{4+}(VIII) = 0.083$ nm

[1] Roman numerals are intended to indicate the coordination of cations by nearest neighbor anions.

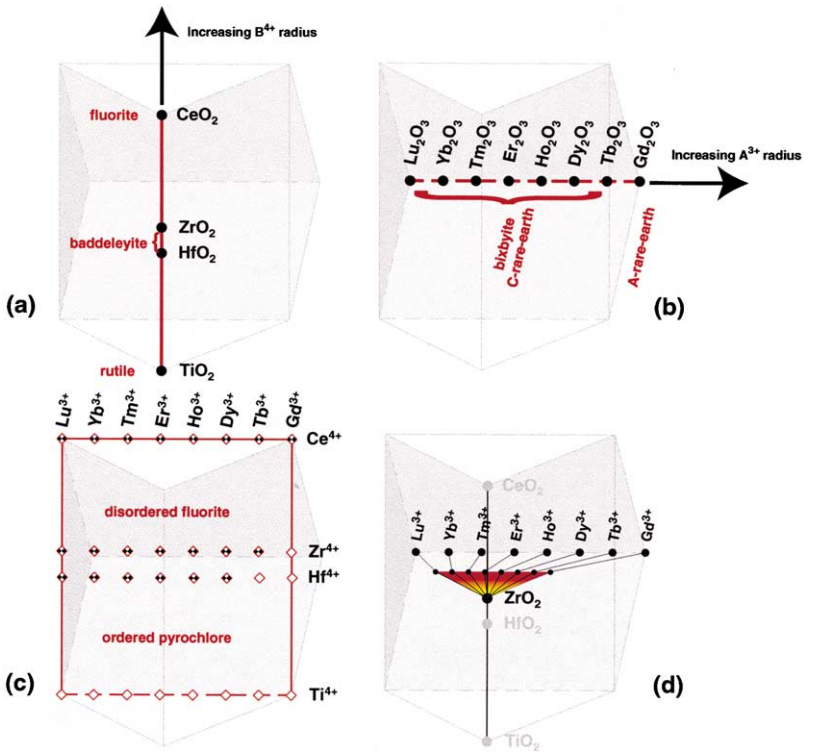

Fig. 1. Schematic diagrams illustrating A_2O_3–BO_2 oxide compositions of interest in discussing possibilities for radiation tolerant ceramics. The vertical axis (a) and horizontal axis (b) are intended to represent increasing ionic radii for B^{4+} and A^{3+} ions, respectively. Compounds highlighted in (c) are $A_2B_2O_7$ oxides, while compositions highlighted in (d) represent rare-earth stabilized cubic zirconia compounds.

and $Zr^{4+}(VIII) = 0.084$ nm in the baddeleyite forms of HfO_2 and ZrO_2. The latter compounds are characterized by monoclinic distortions of the fluorite structure.

The horizontal axis (Fig. 1(b)) represents a series of rare-earth A_2O_3 compounds with increasing A^{3+} radii from left to right. $Lu^{3+}(VI) = 0.0861$ nm is the smallest cation along this axis, while the axis is terminated (somewhat arbitrarily) at Gd^{3+}-$(VI) = 0.0938$ nm (essentially, this axis follows the so-called *rare-earth contraction*, but in the opposite, i.e. expansion direction). Most A_2O_3 sesquioxides in this series form cubic bixbyite (C rare earth) compounds under equilibrium conditions at ordinary temperature and pressure. The exception is Gd_2O_3 which forms a hexagonal, A rare earth compound. All rare earth A^{3+} cations larger than Gd^{3+} also form A rare earth structures. In this paper, we discuss Y-bearing compounds, for which $Y^{3+}(VI) = 0.0900$ nm, which is approximately in the middle of this horizontal axis (nearly coincident with Ho^{3+}).

The middle of the faceted volume (Fig. 1(c)) represents oxide compounds with composition $A_2B_2O_7$. These are so-called 227 oxides whose structures either order to produce the pyrochlore structure (typically cubic with a lattice parameter given by $a' \sim 1$ nm), or disorder to produce a defective fluorite structure (with a reduced lattice parameter of $a \sim 0.5$ nm). In Fig. 1(c), we use open and hatched symbols to indicate that titanate compounds produce ordered pyrochlore structures, while most halfnate and zirconate compounds are disordered fluorites under equilibrium conditions.

Finally, we call attention in Fig. 1(d) to the fact that doping ZrO_2 with a few mole percent of rare earth sesquioxides (A_2O_3) produces the well-known cubic-stabilized zirconia structure (shaded

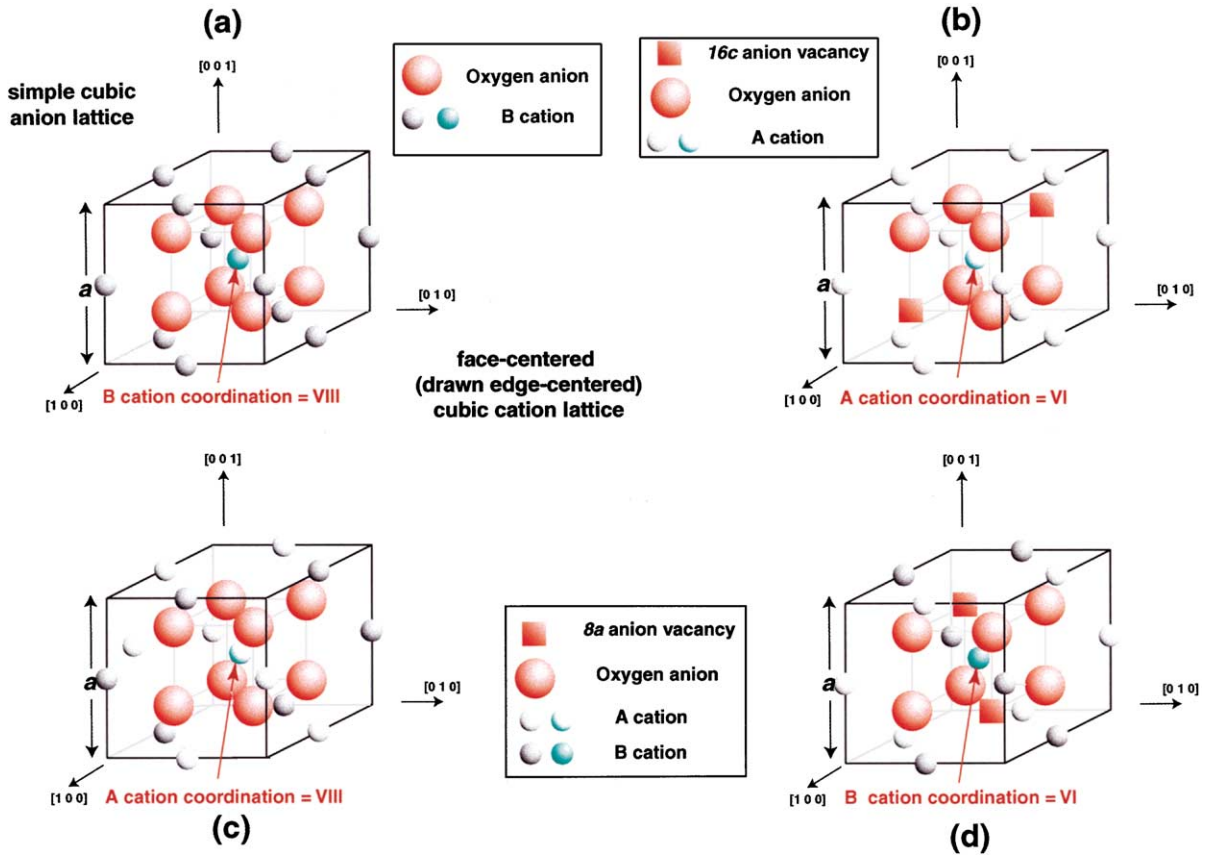

Fig. 2. Important crystallographic characteristics of (a) BO_2 fluorite compounds; (b) A_2O_3 bixbyite compounds; and (c,d) $A_2B_2O_7$ pyrochlore compounds. See text for discussion.

region in Fig. 1(d) with tie lines to the sesquioxide dopants). Cubic-stabilized zirconia is a disordered (often referred to as defective) fluorite structure in which the monoclinic distortion in pure ZrO_2 (baddeleyite) is altered by the introduction of trivalent A^{3+} ions into the lattice along with their charge-compensating oxygen vacancies.

Fig. 2 shows important aspects of the crystal structures corresponding to the A_2O_3–BO_2 compounds from Fig. 1. Fig. 2(a) shows the fluorite structure ($Fm\bar{3}m$) associated with certain BO_2 compounds, particularly CeO_2 in Fig. 1. The anion sublattice is simple cubic (anions occupy the 8c equipoint, using Wycoff notation) with repeat unit $a/2$, while the cations are arranged in a face-centered cubic (fcc) configuration with repeat unit a (cations on the 4a equipoint). The cations are shown shifted by $a/2$ along a cube edge in Fig. 2(a), into edge-centered positions (i.e. on the 4b equipoint) in order to reveal the cation coordination in fluorite: the highlighted cation in the center of the unit cell is surrounded by a cubic arrangement of nearest neighbor anions; hence, the cation coordination is eight (VIII-fold). The overall lattice periodicity is equal to a.

Fig. 2(b) shows one octant of an A_2O_3 cubic bixbyite ($Ia\bar{3}$) compound. The cations are arranged in an *fcc* lattice (shown edge-centered in Fig. 2(c)) with repeat unit a. [2] The idealized anion sublattice is based on a simple cube with repeat unit $a/2$.

[2] Actually, the cation sublattice in bixbyite is distorted from the idealized picture in Fig. 2(b), such that A atoms occupy 8b and 24d equipoints in this space group. These distortions are not important with regard to the discussion presented here.

However, the vacancies associated with anion deficiency in these compounds are ordered so that this sublattice takes on a superperiodicity with repeat unit $a' = 2a$ (consequently, anions occupy equipoint 48e in this space group). The overall periodicity for a bixbyite compound is $a' = 2a$. The highlighted cation at the center of the cell in Fig. 2(b) drawing indicates that the coordination in a bixbyite is VI-fold.

Figs. 2(c) and (d) show the two types of octants in the cubic unit cell of an ordered $A_2B_2O_7$ (227) pyrochlore compound. In an ordered pyrochlore ($Fd\bar{3}m$), such as one of the 227 titanates in Fig. 1(c), the cations assume a periodic arrangement on an fcc lattice (shown as edge-centered in Fig. 2(c) and (d)). The ordered cation arrangement produces a superperiodicity such that the cation sublattice repeat unit is $a' = 2a$ (equipoints 16c and 16d). In a similar fashion, the anion sublattice is superperiodic with repeat unit $a' = 2a$, due to an ordering of the vacant sites (8a equipoint) in these anion-deficient compounds. [3] Thus, each of the cubic cells shown in Fig. 2(c) and (d) (with edge length a) represents one octant of a pyrochlore unit cell. The highlighted A cation in the center of the cell in Fig. 2(c) is surrounded by eight anions, so that the A cation coordination in a pyrochlore is VIII-fold. The highlighted B cation in the center of the cell in Fig. 2(d) is surrounded by six anions, so that the B cation coordination in a pyrochlore is VI-fold.

In a 227 disordered fluorite (i.e. a fully-disordered pyrochlore), the superperiodicity associated with the pyrochlore cation sublattice is absent, as A and B atoms randomly occupy fcc sites and the repeat unit is reduced to a $(= a'/2)$. Similarly, anion vacancies occur with equal frequency on all anion sublattice sites, and this sublattice periodicity is reduced to the $a/2$ $(= a'/4)$ simple cube, as in Fig. 2(a). The overall unit cell periodicity of a disordered fluorite is a and the structure is crystallographically indistinguishable from the ideal, BO_2 fluorite ($Fm\bar{3}m$ with cations and anions on 4a and 8c equipoints, respectively). The average A or B cation coordination in these anion deficient compounds is VII-fold.

Not shown in Fig. 2 are the baddeleyite and rutile structures associated with BO_2 compounds. Baddeleyite is merely a monoclinic distortion of the fluorite structure shown in Fig. 2(a) ($P2_1/c$), while rutile is a tetragonal structure (P4/mnm) with no obvious relationship to any of the structures in Fig. 2.

The hypothesis to be adopted in this paper is that oxides possessing structures closely related to fluorite (such as baddeleyite and bixbyite), and with compositions that readily accommodate disordered atomic arrangements (such as the disordered 227 compounds in Fig. 1(c)), will be most likely to exhibit resistance to radiation-induced amorphization. We propose that these compounds, if not already in a fluorite arrangement, will transform to a disordered fluorite structure upon irradiation, and then persist as crystalline compounds to very high radiation doses.

3.2. Experimental evidence

3.2.1. TiO_2 – rutile

Ion irradiation experiments indicate that the rutile polymorph of TiO_2 is relatively sensitive to radiation-induced amorphization. For instance, Li et al. [9] found that rutile single crystals exposed to 360 keV Xe^{++} ion irradiation at 300 K, were fully amorphized by a dose corresponding to approximately 10 displacements per atom (dpa). Since rutile is crystallographically unrelated to fluorite, the lack of amorphization resistance exhibited by rutile does not violate the hypothesis we proposed at the end of the previous section.

3.2.2. ZrO_2 – baddeleyite

Ion irradiation experiments indicate that the monoclinic polymorph of ZrO_2 transforms to another crystalline phase upon ion irradiation, but amorphization of ZrO_2 is not observed, even at very high ion fluences. For instance, Sickafus et al.

[3] No attempt has been made in Fig. 2(c) and (d) to distinguish between the two types of oxygen positions in a pyrochlore. A 227 pyrochlore is more correctly described as an $A_2B_2O_6O'$ compound with oxygen on 8b and 48f equipoints. The distortions associated with the real oxygen sublattice compared to the idealized sublattice shown in Fig. 2(c) and (d), are of no particular consequence with regard to the discussions found within in this paper.

[10] found that polycrystalline baddeleyite exposed to 340 keV Xe^{++} ion irradiation at 120K, transformed to a higher symmetry phase, either tetragonal or cubic, by a peak dose between 2 and 20 dpa. This crystalline phase persisted without transformation to a peak dose of about 680 dpa. [4] In another experiment using swift heavy ions (in which the electronic stopping exceeded 12 keV/nm), Benyagoub et al. [11] also observed a transformation of baddeleyite, but to a tetragonal polymorph.

The significance of the actual crystal symmetry of the ion-transformed ZrO_2 is not certain at this time. ZrO_2 possesses three polymorphs with increasing temperature and prior to melting: the monoclinic baddeleyite phase below 1420 K; (2) an intermediate temperature tetragonal polymorph between 1440–2640 K; and (3) the cubic, *fluorite*-structured phase from 2640 K to the melting point, $T_m \sim 2950$ K [12]. It seems conceivable that each of these polymorphs may be *visited* by ZrO_2 with increasing radiation damage accumulation, prior to an amorphization transformation at some as yet unknown but large ion dose. Temperature of irradiation and irradiation spectrum (electronic versus nuclear stopping) will play key roles in recovery mechanisms, which will influence the final structure adopted by irradiated ZrO_2. Nevertheless, the crystallography associated with temperature-induced disorder transformations in ZrO_2 suggest that the cubic fluorite polymorph should be stable at the highest levels of accumulated static atomic displacements, prior to an amorphization (melting) transformation.

We anticipate (without proof) similar behavior for another baddeleyite-structured compound, that of HfO_2. We predict that upon displacive radiation damage, HfO_2 will transform from a monoclinic structure to the cubic fluorite structure, and persist to high dose without amorphization.

[4] Ion-induced sputtering effects were not included in the study referenced here, so that it is likely that the peak dose quoted here is an overestimate (see [16] for details). Nevertheless, the peak dose in these experiments most certainly exceeded 100 dpa.

3.2.3. $A_2B_2O_7$ compounds – pyrochlores versus disordered fluorites

We proposed in a previous report [7] that $A_2B_2O_7$ oxides with similar cationic radii, i.e. A^{3+} close to B^{4+} ionic radii, will yield compounds with the best radiation damage performance. In the study referenced above, we compared the radiation response of $Er_2Ti_2O_7$ with $Er_2Zr_2O_7$: $r^{3+(VIII)}/r^{4+(VI)} = 1.66$ versus 1.39, respectively. We found that $Er_2Ti_2O_7$ amorphized by an ion fluence equivalent to a peak dose of just a few ($\sim$3) dpa, while the $Er_2Zr_2O_7$ remained crystalline for all doses tested, i.e. to a peak dose of $\sim$190 dpa [13].

Our calculations [14] suggested that radiation performance would be enhanced if we use compounds with even more similar cationic radii. Thus, for this study we tested the 227 cerate compound $Y_2Ce_2O_7$: $r^{3+(VIII)}/r^{4+(VI)} = 1.33$. We found good amorphization resistance performance for $Y_2Ce_2O_7$, as illustrated by cross-sectional TEM micrographs and microdiffraction patterns in Fig. 3. Heavy ion Xe^{++} irradiations for fluences ranging from 1×10^{19}–5×10^{20} Xe/m^2 produced no evidence for amorphization of this as-synthesized, disordered fluorite compound. Microdiffraction patterns shown to the right of each micrograph in Fig. 3 indicate that the irradiated layers remain crystalline and possess a crystal structure equivalent to the fluorite substrate, over the ion fluence range tested (the peak nuclear displacement dose at the highest ion fluence used in these experiments was $\sim$180–190 dpa). Voids or bubbles (perhaps containing Xe) were observed at the highest ion fluence (Fig. 3(b)), but this is believed to be an artifact associated with the minimal ion range obtainable in these irradiation experiments (a fluence of 5×10^{20} Xe/m^2 represents 50 monolayers of implanted Xe, which over a target depth of 100 nm, produces a considerable change in target composition).

Wang et al. [15] also studied the ion irradiation performance of compounds ranging in composition from $Gd_2Ti_2O_7$ to $Gd_2Zr_2O_7$: $r^{3+(VIII)}/r^{4+(VI)} = 1.74$ and 1.46, respectively. Not only did they find that amorphization resistance improved as the composition was varied from $Gd_2Ti_2O_7$ to $Gd_2Zr_2O_7$, but they also observed that compounds close to the $Gd_2Ti_2O_7$ end-member composition

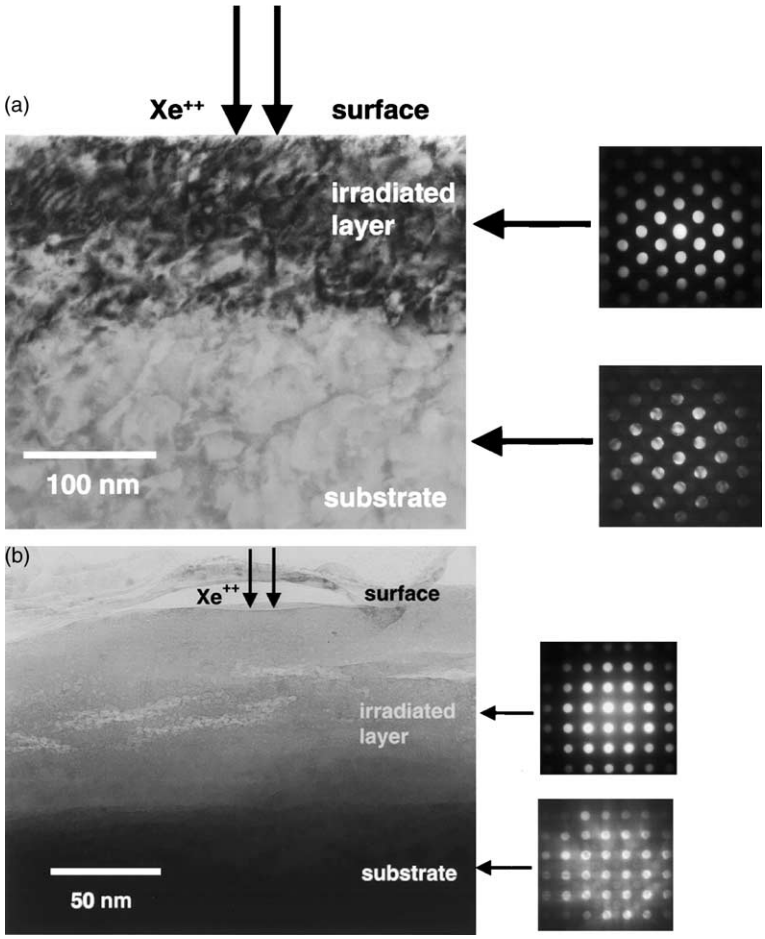

Fig. 3. Cross-sectional TEM micrographs obtained from $Y_2Ce_2O_7$ cerates irradiated with 350 keV Xe^{++} ions at cryogenic temperature to the following fluences: (a) 1×10^{20} Xe/m^2 and (b) 5×10^{20} Xe/m^2. Also shown in (a,b) are microdiffraction patterns obtained from the irradiated layer and the substrate in each sample. Electron beam directions ($\vec{\mathbf{B}}$) are given by (a) $\langle 1\,1\,0 \rangle$; (b) $\langle 1\,0\,0 \rangle$.

transformed to the disordered fluorite structure (with reduced lattice parameter) prior to amorphization. This result seems to imply that there is no particular significance to be ascribed to the fluorite crystal structure with regard to amorphization resistance. However, our calculations suggest that the chemistry of $Gd_2Ti_2O_7$ is not conducive to accommodation of point defects (due to the vast disparity between cationic radii for Gd^{3+}(VIII) versus Ti^{4+}(VI)), so that amorphization resistance cannot be anticipated in this compound. Amorphization resistance is determined by an intricate balance between crystal structure and favorable chemistry.

3.2.4. A_2O_3 – bixbyite

As part of this study, we performed 300 keV Xe^{++} ion irradiations of bixbyite compounds, specifically the compound Dy_2O_3. Fig. 4 shows cross-sectional TEM micrographs of the irradiated microstructure in Dy_2O_3, along with microdiffraction patterns from the substrate and irradiated layer. By an ion fluence of 1×10^{20} Xe/m^2 (Fig. 4(a)), the diffraction pattern is observed to change relative to the substrate (the peak displacement damage at this ion fluence is ~44 dpa). While the substrate diffraction pattern can be indexed consistent with a body-centered cubic bixbyite structure ($a' = 1.0665$ nm), the diffraction pattern from

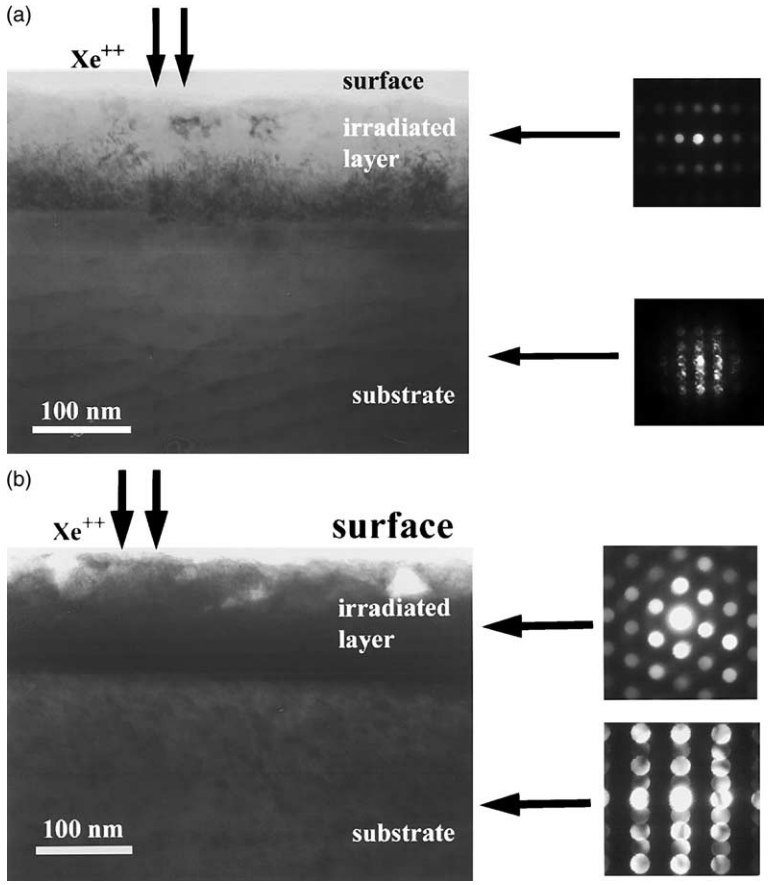

Fig. 4. Cross-sectional TEM micrographs obtained from Dy_2O_3 (bixbyite) irradiated with 300 keV Xe^{++} ions at cryogenic temperature to the following fluences: (a) 1×10^{20} Xe/m^2 and (b) 5×10^{20} Xe/m^2. Also shown in (a,b) are microdiffraction patterns obtained from the irradiated layer and the substrate in each sample. Electron beam directions ($\vec{\mathbf{B}}$) are given by (a) $\langle 211 \rangle$; (b) $\langle 211 \rangle$ substrate, $\langle 110 \rangle$ implanted region.

the irradiated layer indexes as an fcc Bravais lattice with a lattice parameter equal to one-half that of the substrate ($a = 0.53325$ nm). This observation is consistent with a radiation-induced disordering process in which the anion superlattice associated with bixbyite is destroyed and the material adopts a disordered (anion deficient) fluorite structure. Nevertheless, this disordered fluorite structure persists without suffering an amorphization transformation to at least a peak dose of more than 200 dpa (Fig. 4(b)). Voids (or bubbles) are observed in the irradiated microstructure, but the fluorite crystal structure appears to remain intact. We also observed that the irradiated layer became polygonized at the highest Xe ion fluence (Fig. 4(b)), so that the irradiated layer does not maintain an orientation relationship with the substrate. This was also observed in irradiations of cubic stabilized ZrO_2 [16] and in rutile-structured TiO_2 [9]. Work is in progress to better understand this phenomenon.

3.2.5. A_2O_3 – doped ZrO_2 (cubic-stabilized zirconia)

Previous investigations of radiation damage behavior in cubic-stabilized zirconia have revealed high radiation tolerance for this disordered fluorite structure (see for example [10,17,18]). Amorphization of cubic-stabilized zirconia was observed in one ion irradiation study using Cs^+ ions [19].

However, this result is likely a chemical effect associated with a large change in local composition due the incorporation of a very high concentration of implanted Cs^+ ions. In most ion irradiation studies of cubic-stabilized zirconia, no amorphization transformation is observed to peak ion doses equivalent to about 200 dpa.

4. Summary

Our ion irradiation experiments on $Y_2Ce_2O_7$ indicate that this 227 cerate is not amorphized to displacement doses equivalent to ~180–190 dpa. In experiments on $La_2Ce_2O_7$, we found similar results (not presented here [20]). Additionally, irradiations of the bixbyite compound Dy_2O_3 indicate no amorphization transformation to similar dose. The Dy_2O_3 bixbyite compound does transform to a disordered fluorite by a dose of ~40 dpa. We also found similar results for the following bixbyite mixtures: $(Dy_{1.5}Er_{0.5})O_3$, $(Dy_{1.0}Er_{1.0})O_3$, $(Dy_{0.5}Er_{1.5})O_3$ and Er_2O_3 (results not presented here [21]).

Based on the findings presented here and results from previous studies, we have developed in this paper a prediction regarding the radiation damage behavior of certain oxides. Namely, we proposed that A_2O_3–BO_2 compounds that possess structures either equivalent to or related to the fluorite structure, will resist amorphization to high displacive radiation dose, provided that the ionic radii of the A and B constituents are not highly disparate.

In Fig. 1, we presented a composition diagram representing potentially radiation tolerant oxide mixtures. The map includes titanates, though we predict that titanates will not generally perform well in a radiation environment. Some titanates do not possess structures similar to fluorite (e.g. rutile), while other Ti-bearing mixtures are not favorable because the small size of the Ti^{4+} ion yields A^{3+}/Ti^{4+} radius ratios that are unacceptably large. The transition to good radiation damage behavior presumably occurs near the middle of the BO_2 axis in Fig. 1, perhaps at Hf^{4+} or between Hf^{4+} and Zr^{4+}.

The diagram in Fig. 1 is not all-inclusive with regard to radiation tolerance characteristics. In fact, A^{3+} ions with larger radii than shown here can yield radiation tolerant compounds (e.g. La^{3+} in $La_2Ce_2O_7$). Other important A^{3+} ions not shown in Fig. 1 may include Ce^{3+}, Pu^{3+} and Am^{3+}. Larger B^{4+} ions may also be found to produce highly radiation tolerant A_2O_3–BO_2 compounds. Examples include Th^{4+}, U^{4+} and Pu^{4+}. Nor are these concepts limited to 3+ and 4+ valence cations. Many divalent and pentavalent cations are compatible with the structures discussed in this paper. For instance, CaO with Ca^{2+} cations is an excellent stabilizer for the cubic phase of zirconia. Experiments have shown that calcia-stabilized zirconia is highly resistant to amorphization [10,18].

Finally, we speculate that compounds with superstructures related to fluorite, such as bixbyite and pyrochlore, will transform to disordered fluorite structures upon irradiation. Then, provided compound chemistry is favorable to the accommodation of lattice disorder, these compounds will persist as crystalline fluorites to very high radiation doses.

Acknowledgements

This work was sponsored by the US Department of Energy, Office of Basic Energy Sciences, Division of Materials Sciences.

References

[1] H. Matzke, J. van Geel, Radwaste Magazine 3 (1996) 71.
[2] W.J. Weber, R.C. Ewing, C.R.A. Catlow, T. Diaz de la Rubia, L.W. Hobbs, C. Kinoshita, H. Matzke, A.T. Motta, M. Nastasi, E.K.H. Salje, E.R. Vance, S.J. Zinkle, J. Mater. Res. 13 (6) (1998) 1434.
[3] T. Shikama, K. Yasuda, S. Yamamoto, C. Kinoshita, S.J. Zinkle, E.R. Hodgson, J. Nucl. Mater. 272 (1999) 560.
[4] L.W. Hobbs, F.W. Clinard Jr., S.J. Zinkle, R.C. Ewing, J. Nucl. Mater. 216 (1994) 291.
[5] C. Kinoshita, S.J. Zinkle, J. Nucl. Mater. 233–237 (1996) 100.
[6] F.W. Clinard Jr., L.W. Hobbs, in: R.A. Johnson, A.N. Orlov (Eds.), Physics of Radiation Effects in Crystals, Elsevier, Amsterdam, 1986, p. 387.
[7] K.E. Sickafus, L. Minervini, R.W. Grimes, J.A. Valdez, M. Ishimaru, F. Li, K.J. McClellan, T. Hartmann, Science 289 (2000) 748.
[8] R.D. Shannon, Acta Cryst. A 32 (1976) 751.

[9] F. Li, M. Ishimaru, P. Lu, I.V. Afanasyev-Charkin, K.E. Sickafus, Nucl. Instr. and Meth. B 166–167 (2000) 314.
[10] K.E. Sickafus, H. Matzke, T. Hartmann, K. Yasuda, J.A. Valdez, P. Chodak III, M. Nastasi, R.A. Verrall, J. Nucl. Mater. 274 (1999) 6.
[11] A. Benyagoub, F. Levesque, F. Couvreur, C. Gibert-Mougel, C. Dufour, E. Paumier, Appl. Phys. Lett. 77 (20) (2000) 3197.
[12] R. Stevens, Zirconia and Zirconia Ceramics, Magnesium Elecktron Ltd., Twickenham, United Kingdom, 1986.
[13] K.E. Sickafus, L. Minervini, R.W. Grimes, J.A. Valdez, T. Hartmann, Rad. Eff. Def. Sol. 155 (2001) 133.
[14] L. Minervini, R.W. Grimes, K.E. Sickafus, J. Am. Ceram. Soc. 83 (8) (2000) 1873.
[15] S.X. Wang, B.D. Begg, L.M. Wang, R.C. Ewing, W.J. Weber, K.V. Godivan Kutty, J. Mater. Res. 14 (12) (1999) 4470.
[16] I.V. Afanasyev-Charkin, K.E. Sickafus, J. Nucl. Mater., submitted for publication.
[17] N. Yu, K.E. Sickafus, P. Kodali, M. Nastasi, J. Nucl. Mater. 244 (1997) 266.
[18] K. Yasuda, M. Nastasi, K.E. Sickafus, C.J. Maggiore, N. Yu, Nucl. Instr. and Meth. B 136–138 (1998) 499.
[19] L.M. Wang, S.X. Wang, R.C. Ewing, Phil. Mag. Lett. 80 (5) (2000) 341.
[20] J.A. Valdez, K.E. Sickafus, 2001, unpublished results.
[21] J.R. Williams, K.E. Sickafus, 2001, unpublished results.
[22] J.F. Ziegler, J.P. Biersack, U. Littmark, The Stopping and Range of Ions in Solids, Pergamon Press, New York, 1985.